Technical Note

Time-Resolved Three-Dimensional Phase-Contrast MRI

Michael Markl, PhD,[1]* Frandics P. Chan, MD, PhD,[1] Marcus T. Alley, PhD,[1] Kris L. Wedding, PhD,[1] Mary T. Draney, MS,[2] Chris J. Elkins, PhD,[2] David W. Parker, MS,[2] Ryan Wicker, PhD,[3] Charles A. Taylor, PhD,[2] Robert J. Herfkens, MD,[1] and Norbert J. Pelc, ScD,[1]

Purpose: To demonstrate the feasibility of a four-dimensional phase contrast (PC) technique that permits spatial and temporal coverage of an entire three-dimensional volume, to quantitatively validate its accuracy against an established time resolved two-dimensional PC technique to explore advantages of the approach with regard to the four-dimensional nature of the data.

Materials and Methods: Time-resolved, three-dimensional anatomical images were generated simultaneously with registered three-directional velocity vector fields. Improvements compared to prior methods include retrospectively gated and respiratory compensated image acquisition, interleaved flow encoding with freely selectable velocity encoding (*venc*) along each spatial direction, and flexible trade-off between temporal resolution and total acquisition time.

Results: The implementation was validated against established two-dimensional PC techniques using a well-defined phantom, and successfully applied in volunteer and patient examinations. Human studies were performed after contrast administration in order to compensate for loss of inflow enhancement in the four-dimensional approach.

Conclusion: Advantages of the four-dimensional approach include the complete spatial and temporal coverage of the cardiovascular region of interest and the ability to obtain high spatial resolution in all three dimensions with higher signal-to-noise ratio compared to two-dimensional methods at the same resolution. In addition, the four-dimensional nature of the data offers a variety of image processing options, such as magnitude and velocity multi-planar reformation, three-directional vector field plots, and velocity profiles mapped onto selected planes of interest.

Key Words: phase contrast MRI; flow; cardiovascular MRI; velocity mapping; flow quantification
J. Magn. Reson. Imaging 2003;17:499–506.

CARDIAC MAGNETIC RESONANCE imaging (MRI) is an essential tool in the diagnosis, monitoring, and treatment of cardiac diseases, and has the potential of evaluating both anatomy and function of the cardiovascular system. Traditionally, MRI imaging of flow is accomplished using methods that resolve two spatial dimensions (two-dimensional) in individual slices. The temporal dimension can be assessed using techniques such as k-space segmentation in combination with retrospectively or prospectively gated data acquisition (CINE imaging). To extend the spatial coverage of these techniques, a three-dimensional spatial volume can be imaged in multi-slice mode (1–6). Typically, multiple slices are acquired sequentially using several breath-held measurements. Disadvantages of these techniques include the inconsistent and incomplete spatial volume coverage caused by gaps between adjacent slices, imperfect slice profiles, and breath-hold misregistration. Further, it is demanding to obtain high spatial resolution in the slice direction due to the intrinsically lower signal-to-noise ratio (SNR) of two-dimensional vs. three-dimensional spatial encoding. As a result, it is difficult to fully resolve and analyze flow patterns or wall motion.

Alternatively, three-dimensional spatial encoding offers the possibility of isotropic high spatial resolution, and thus the ability to measure and visualize the temporal evolution of complex flow and motion patterns in a three-dimensional volume. To exploit the advantages of a volumetric vs. planar-approach, we implemented a technique that can produce time-resolved, three-dimensional PC images. Due to the four-dimensional character of the acquisition (three spatial and one temporal dimension), we refer to this method as 4D-Flow.

[1]Department of Radiology, Stanford University, Stanford, California.
[2]Department of Mechanical Engineering, Stanford University, Stanford, California.
[3]Mechanical and Industrial Engineering Department, University of Texas at El Paso, El Paso, Texas.
Contract grant sponsor: National Institutes of Health; Contract grant numbers: R01 HL46347 and P41 RR09784; Contract grant sponsor: DFG Fellowship; Contract grant sponsor: Kyle Mann grant.
Parts of this work were presented at ISMRM 2002.
*Address reprint requests to: M.M., Stanford University, Department of Radiology, Lucas MRI/S Center, 1201 Welch Road, Room P 284, Palo Alto, CA 94304. E-mail: markl@s-word.stanford.edu
Received July 18, 2002; Accepted November 21, 2002
DOI 10.1002/jmri.10272
Published online in Wiley InterScience (www.interscience.wiley.com).

The method obtains, for each pixel within a three-dimensional volume at each measured time point of the cardiac cycle, anatomical and three-directional velocity information. In comparison to some previously reported implementations (7–14), considerably shorter TEs and TRs were accomplished using minimal TE flow encoding strategies (6). As a result, the temporal resolution is improved significantly for similar total acquisition times.

Techniques similar to our 4D-Flow method have been applied to the qualitative assessments of flow patterns in the great vessels (7), the thoracic aorta (8), the left ventricle and the outflow tract (10), the left atrium (12), and the aortic valve (14). The work presented in this paper is closely related to results reported previously by Kozerke et al (14). The major advantages of our implementation include retrospectively gated image acquisition, and thus complete coverage of the entire cardiac cycle. Also, our method permits a flexible trade-off between temporal resolution and total scan time. In addition, different velocity encoding (*venc*) could be selected along each spatial direction to adapt the velocity encoding to non-isotropic flow characteristics. Because the total scan time is relatively long, methods must be incorporated to control respiratory motion (15,16). This was done by respiratory compensation in which the phase encode ordering was adjusted to minimize respiratory artifacts.

The four-dimensional data can be reformatted onto freely selectable sub-volumes, planes, or regions of interest (ROIs). Several previously described processing techniques (17,18) can then be used to analyze and visualize the four-dimensional flow results, including velocity waveforms and vector field plots mapped onto reformatted planes, as will be demonstrated below.

The purpose of this paper is to demonstrate the feasibility of our 4D-Flow implementation, to quantitatively validate its accuracy against an established time resolved two-dimensional PC technique (2D-PC) with a well-defined phantom, and to explore advantages of the approach with regard to the four-dimensional nature of the data and the complete coverage of an entire three-dimensional volume.

MATERIALS AND METHODS

All measurements were performed on a 1.5-T system (Signa CV/i, GE, Milwaukee, WI, G_{max} = 40 mT/m, rise time = 268 μsec). The pulse sequence for four-dimensional flow data acquisition consisted of a radiofrequency (rf)-spoiled gradient-echo sequence with velocity encoding along all three spatial directions. Measurements were retrospectively gated to the electrocardiogram (ECG) cycle in order to generate a CINE series of three-dimensional data sets. Minimal TEs were achieved by designing gradient waveforms for flow encoding according to Bernstein et al (6). In order to minimize artifacts in phase-difference images related to subject motion, the different flow encodes were kept as close together as possible in time.

A schematic representation of the data acquisition strategy is shown in Figure 1. Within each cardiac cycle, one k_y (phase encoding) step was employed for all acquired time frames. All four flow encodes and a selectable number n_{kz} of k_z (slice-encodings) were interleaved. This results in a flexible trade-off between temporal resolution T_{Res} of the CINE images and total acquisition time T_{Acq}, given by:

$$T_{Res} = 4TRn_{kz}, \quad (1)$$

$$T_{Acq} = N_{ky} \frac{N_{kz}}{n_{kz}} T_{ECG} \quad (2)$$

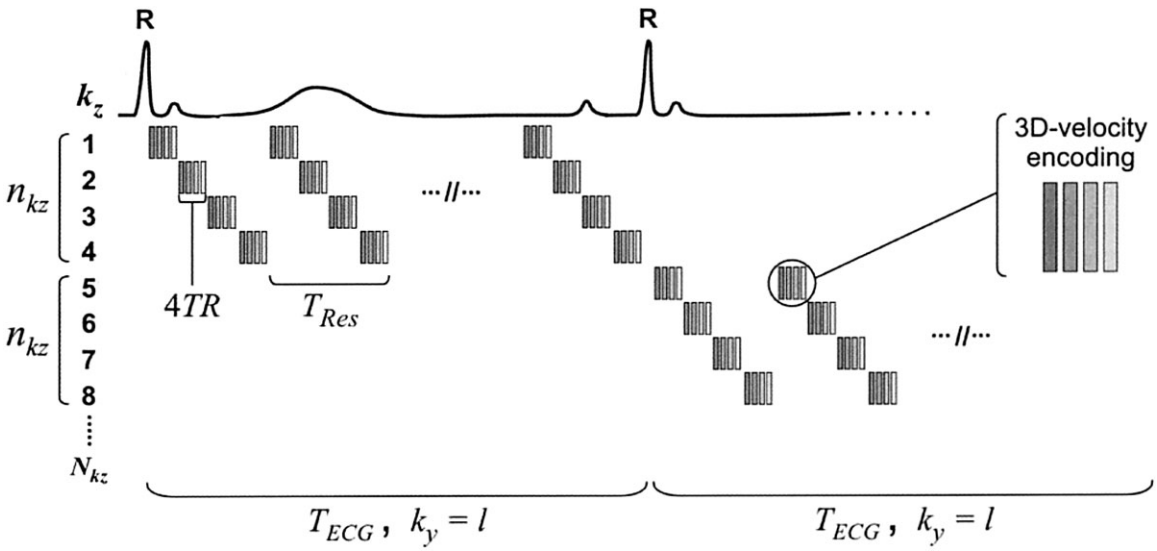

Figure 1. Phase-encoding scheme for an ECG-gated 4D-Flow acquisition with flow encoding along all spatial directions and a selected number of n_{kz} = 4 slice-encodes for each cardiac cycle. Two adjacent ECG-cycles for the l^{th} k_y phase encoding step and the first two subsections (n_{kz}) of a total of N_{kz} slice encodes are shown. Three-directional velocity encoding is illustrated by the gray shaded bars representing pulse sequences with different first moments but otherwise identical parameters.

with N_{ky} = total number of phase-encoding steps, N_{kz} = total number of slice-encoding steps, and T_{ECG} = average cardiac period.

During the acquisition, the collected data were transferred and stored on a remote computer using a bus adapter connected to the backplane of the scanner (e.g., 19). At the completion of the scan, the remote computer was used to temporally sort, interpolate, and reconstruct the data. The resulting images were then transferred and installed in the image database of the scanner.

To evaluate the quantitative accuracy of the 4D-Flow technique in a controlled environment, velocity measurements were compared with those acquired by a conventional two-dimensional PC CINE technique on a pulsatile flow phantom. The phantom consisted of a stiff U-shaped tube. A stenosis and a parallel bypass conduit were placed in the forward-flow limb. The flow tubes and bypass conduit had diameters of 19.1 and 15.9 mm, respectively. The stenosis was a tapered 75% reduction in cross-sectional area, with a length of 3.2 mm (see Fig. 2). The physical model was built layer by layer within a photoreactive resin that was spot-cured by controlled laser light. To mimic physiologic arterial flow in medium to large vessels, a pump was used to drive pulsatile flow through the phantom at a rate of 70 cycles per minute, with a peak flow of 3 liters/minute and a systolic fraction of 50%. A simulated ECG signal triggered by the pump was used for gating.

For the 4D-Flow acquisition, a raw data matrix of $N_{kx} \times N_{ky} \times N_{kx} = 256 \times 256 \times 44$ and $n_{kz} = 4$ resulted in a temporal resolution of T_{Res} = 92.8 msec and a total scan time of T_{Acq} = 18 minutes (echo time [TE] = 2.2 msec, repetition time [TR] = 5.8 msec, $\alpha = 15°$). The three-dimensional volume was acquired as an axial slab with an in-plane field of view (FOV) of 240 mm and a slab thickness of 132 mm (spatial resolution = [$(0.94 \times 0.94 \times 3)$mm^3]) including the stenosis and the bypass conduit of the phantom.

For comparison, two-dimensional PC CINE MRI was performed in axial planes transecting the phantom. The same in-plane matrix, slice thickness, and FOV as for the four-dimensional flow acquisition were used. Measurements were carried out for two sets of two-dimensional scans with different temporal resolutions of 72 msec and 43 msec referred to below as 2D-PC(1) and 2D-PC(2), respectively. A *venc* of 100 cm/second was used for all directions and all scans.

The geometry of the phantom and the position of the three-dimensional volume and slice planes locations for the two-dimensional PC scans are depicted in Figure 2. Data for five axial planes were reformatted from the four-dimensional flow data set and compared with the corresponding two-dimensional PC results (see Fig. 2, slice planes I–V). Mean and velocity profiles $v_z(x,y)$ were calculated and analyzed. Note that two-dimensional PC slice locations I and V were positioned outside the volume covered by the four-dimensional flow scan to generate boundary conditions for future analysis using computational fluid dynamics. For the analysis presented here, those slice plane locations were compared to the outermost sections of the three-dimensional volume covered by the 4D-Flow scan.

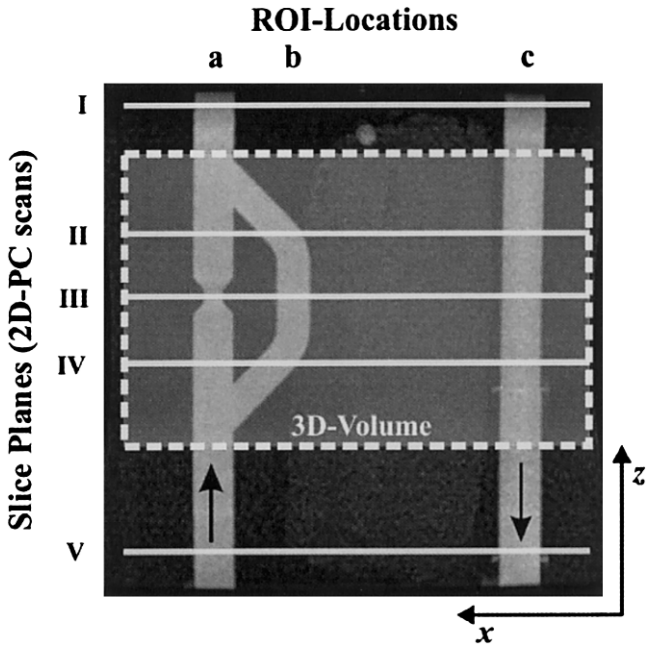

Figure 2. Geometry of the phantom (coronal [*x*-*z*]-plane, maximum intensity projection [MIP] image) used for the validation of the 4D-Flow technique. The black arrows show the direction of pulsatile flow. The prescription of the three-dimensional volume for the 4D-Flow acquisition is indicated by the gray shaded area. Corresponding two-dimensional PC (2D-PC) slice plane locations are shown as thick horizontal lines at *z*-positions I–V. ROI locations a–c indicate the different tubes used for evaluating ($\bar{v}_z$). A stenosis and a bypass were included in the left-most tube to simulate a blood vessel stenosis and a bypass graft, and to generate spatial and temporal modifications in flow patterns. Two-dimensional PC slice locations I and V were compared to outermost slices of the three-dimensional volume.

To demonstrate the high spatial resolution attainable with our technique, an additional data set (FOV = 160 mm, matrix = $N_{kx} \times N_{ky} \times N_{kx} = 256 \times 224 \times 40$, 40-mm slab thickness, $n_{kz} = 4$, TE =2.7 msec, TR = 7.2 msec, $\alpha = 15°$) with a spatial resolution of $(0.63 \times 0.71 \times 1)$mm^3 was acquired. The three-dimensional volume included the stenosis in the phantom.

In order to correct for background phase shifts due to eddy currents and system imperfections other than gradient inhomogeneities, the measured phase-difference images for each experiment were referenced to those for a time frame with no flow but otherwise identical parameters.

The feasibility of imaging the human heart with the 4D-Flow technique was demonstrated in 10 subjects (age range 13 to 70). Informed consent was obtained from all subjects. In a typical protocol, the four-dimensional flow examination was preceded by a contrast-enhanced MR angiogram that included intravenous gadolinium contrast agent administration (gadopentate dimeglumine; Magnevist, Berlex, Wayne, NJ) at a 0.2 mmol/kg dose. Contrast was delivered as a bolus (injection rate 2–3 mL/second) and initially used for the routine MR angiogram. The 4D-Flow scan was performed directly after the MR angiogram to benefit

from the contrast agent remaining in the blood pool. Previous experience with three-dimensional CINE imaging shows that three-dimensional slab excitation methods greatly benefit from the use of contrast media, while constant infusion during the scan is not essential (20,21). Two to five minutes after injection, 4D-Flow imaging was performed with a 320–360 mm FOV and a 256 × 160 matrix in axial orientation. Thirty-two to 40 slice-encodes were acquired in a slab thickness of 160 mm, resulting in a spatial resolution of (1.25 – 1.4 × 2.0 – 2.25 × 4.0 – 5.0)mm^3 covering a volume of interest in the thorax (adjusted on a patient-to-patient basis and depending on the examined pathology) that included most of the heart from base to apex and a portion of the great vessels. Because velocities are typically higher for blood flow along the long axis of the heart, velocity sensitivities were adjusted accordingly. For axial slab orientation, in-plane velocity components in the range of 50–100 cm/second occur, for example, in pulmonary arteries or the left ventricular outflow tract (see also Fig. 7). Therefore, *vencs* corresponding to blood flow within the axial planes were usually lower (100–150 cm/second) than for the through-slab direction (150–250 cm/second).

In order to further reduce TE and TR, a fractional echo readout utilizing 70% of the full echo was used for all experiments. Depending on the selected *vencs*, the 4D-Flow imaging protocol (α = 15°, BW = 62.5 kHz) employed a TE of 1.7–2.0 msec and TR of 4.4–4.9 msec. Four slice encodes (n_{kz} = 4) were interleaved per cardiac cycle, resulting in a temporal resolution of 70.6–78.4 msec. The human data were collected during free breathing using respiratory compensation with total scan times on the order of 12–18 minutes, depending on the heart rate. The respiration was monitored with bellows to generate real-time estimates of the phase in the respiration cycle, which was then translated into phase encoding amplitudes such that the final data set appeared to be collected during a single respiration cycle.

For each slice an independent correction for background phase shifts was performed based on the assumption that little or no flow occurs in late diastole and any apparent non-zero phase-difference values are due to eddy currents and other system imperfections. Therefore, for each slice, a plane was fitted to phase-difference images during late diastole and the resulting fit was subtracted from the measured phase-difference images for that slice.

The four-dimensional data sets were evaluated with visualization software developed at our institution.

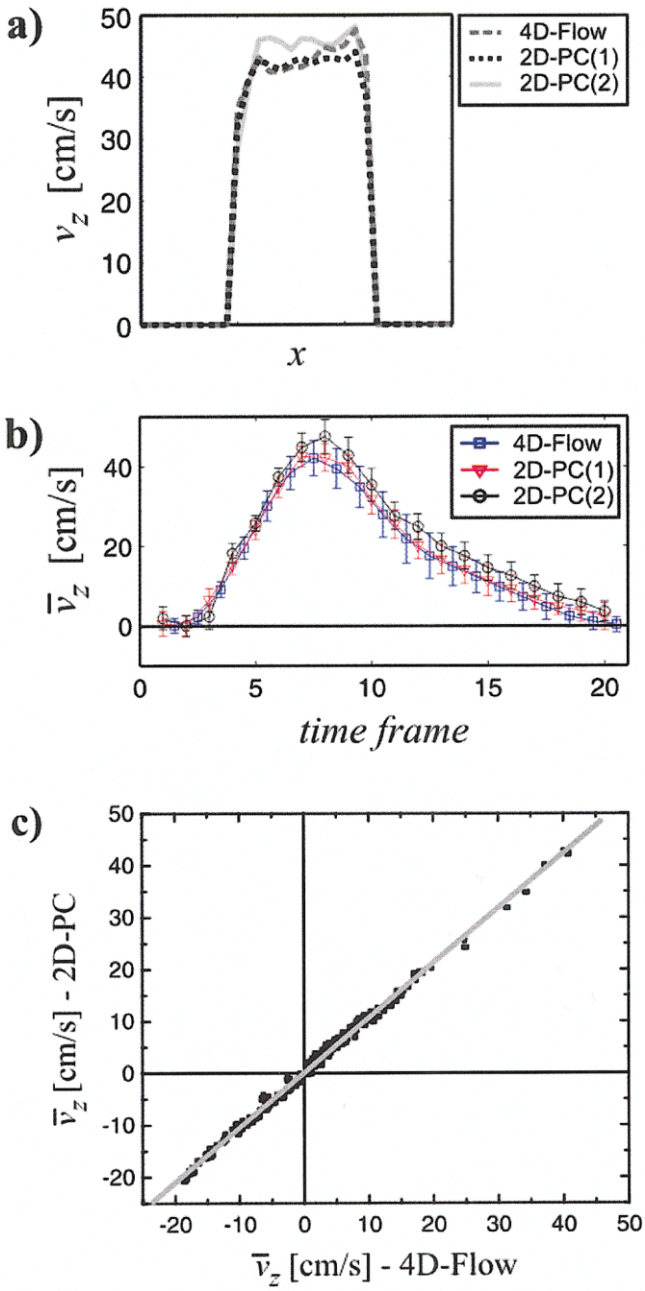

Figure 3. Selected results for the validation of the 4D-Flow technique. **a:** Comparison of velocity profiles $v_z(x)$ at peak flow for the two-dimensional PC slice location III (see Fig. 2) and a ROI location corresponding to the stenosis (IIIa). The x-coordinate is given in units of pixels, and extends over a width of 30 pixels **b:** Selected ($\bar{v}_z$) waveform at the same location (IIIa). **c:** Cumulative correlation for through-plane velocities. Only the plot for correlation of the four-dimensional flow results with 2D-PC(1) is shown. The solid line represents the result of a linear regression of both methods. [Color figure can be viewed in the online issue, which is available at www.interscience.wiley.com.]

RESULTS

Validation

Figure 3 and Table 1 summarize the results of the phantom validation of the 4D-Flow technique. Excellent agreement was found for all measured quantities, such as velocity profiles, mean velocity waveforms, and correlation of mean velocities. As an example, cross-sectional velocity profiles at peak flow at the level of the stenosis are shown in Figure 3A. Velocities $v_z(x)$ were extracted along the central line through the tube at location IIIa, as depicted in Figure 2. Similarly, close agreement between four-dimensional flow and two-dimensional PC measurements were obtained at all other levels. As expected, significantly higher velocities were

Table 1
Results of Linear Regression ($y = \bar{v}_z$-2D-PC, $x = \bar{v}_z$-4D-Flow) of 4D-Flow Versus Both Two-dimensional PC(2D-PC(1) and 2D-PC(2))

Parameter	Fit results ($y = ax + b$, $N = 254$)	
	4D-Flow vs. 2D-PC(1)	4D-Flow vs. 2D-PC(2)
Slope *a*	1.057 ± 0.005	1.116 ± 0.006
Intercept *b*	0.099 ± 0.048	0.140 ± 0.070
Correlation *r*	0.99	0.99

Correlation was performed for mean velocities $\bar{v}_z$, independently averaged over each ROI a-c and each location I-V and each time frame.

observed in the stenosis as compared to other locations. Examples of the temporal evolution of velocities measured with both 4D-Flow and two-dimensional PC at the level of the stenosis are shown in Figure 3B. The graph shows the mean $\bar{v}_z$ for 4D-Flow (squares) and the two two-dimensional PC (triangles and circles) scans as a function of time. Figure 3C shows the correlation of mean velocities $\bar{v}_z$ at all ROI locations a–c within all slice plane locations I–V measured with 4D-Flow and two-dimensional PC. Data points represent mean through-plane velocities (independently averaged over each ROI a–c, slice location I–V, and time frame). Results of a linear regression between 4D-Flow and two-dimensional PC are listed in Table 1.

Visualization

Various data processing strategies that illustrate the advantage of the complete temporal and spatial coverage of the four-dimensional data are presented in this section. The boundaries of the flow channels were segmented using thresholding, and velocity values for pixels outside the boundary were set to zero. Flow through the stenosis was reformatted to the coronal (*x*-*z*) plane. The low resolution four-dimensional flow data (3-mm slice thickness) was used to generate three-dimensional surface plots of the through-plane velocities in the central plane through the stenosis (Fig. 4). Characteristic flow features, such as acceleration of the fluid as it enters the stenosis, as well as relatively plug-like flow through the narrowing, can be identified. In addition, reverse flow or recirculation is observable adjacent to the forward jet distal to the stenosis (arrows).

The temporal evolution of pulsatile flow through the phantom can be effectively displayed as a movie of vector field maps. A more static visualization mode is demonstrated in Figure 5, which shows five time frames of a vector field animation during peak flow. Formation of the jet at the stenosis can be clearly identified. It should be noted that similar images could be generated in arbitrary plane orientations retrospectively.

In order to visualize data from the entire three-dimensional volume covered by the four-dimensional flow acquisition, vector field plots were overlaid onto three orthogonal freely selectable planes that cut through the measured volume along the main (*x*, *y*, *z*) axes. In addition, the measured velocities were reformatted onto these selected planes and color-coded according to their *z*-components. Figure 6 shows a resulting three-dimensional graph for the time frame with peak flow generated from the high resolution data set.

Human Studies

As an example of the robust image quality obtained from human studies, Figure 7 shows the anatomic and

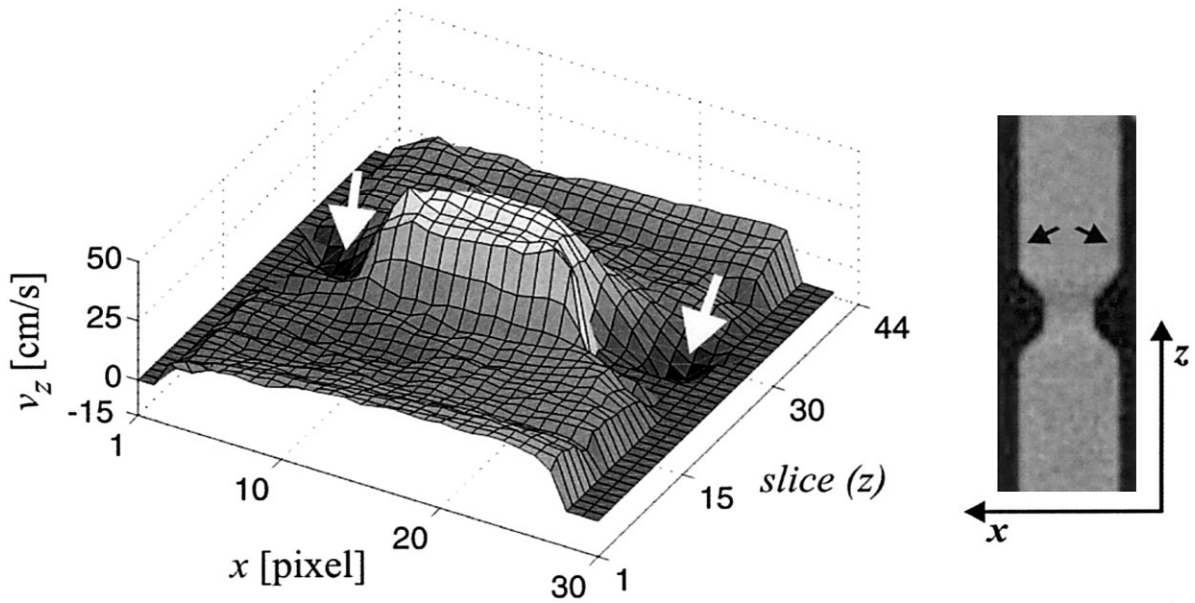

Figure 4. Three-dimensional visualization of velocity profiles at peak flow (left) reformatted onto the coronal (*x*-*z*) plane. The graph represents flow characteristics in the left-most tube. Note the peak flow during passage through the stenosis and flow separation, and reverse flow just distal to the stenosis (white arrows). The area covered by the three-dimensional plot and the locations of reverse flow (black arrows) are indicated in the MIP image of the stenosis on the right.

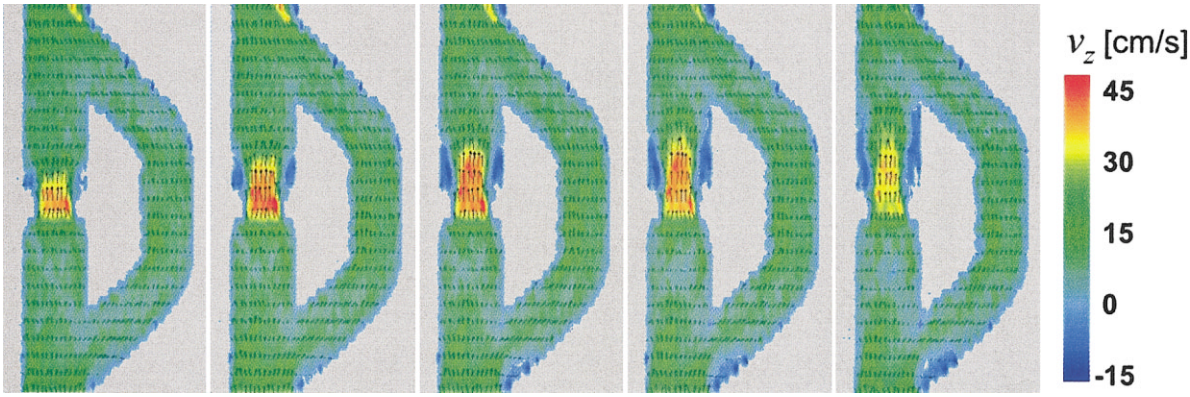

Figure 5. Temporal evolution of color-coded velocity vector fields. Data shown here were collected with a spatial resolution of (0.94 × 0.94 × 3)mm^3. Subsets of the three-dimensional volume, including the stenosis and the bypass conduit, are shown for five out of 20 reconstructed time frames that represent the passage of peak flow through the stenosis. Three-directional velocity vectors were color-coded according to the magnitude of the velocity. Reverse flow can be identified by blue colored areas distal to the stenosis.

three-directional flow information for a single axial slice and single time frame from the study of a healthy volunteer.

Similar visualization techniques, as demonstrated in Figures 5 and 6, were applied to in vivo data. Although only principal axis reformations were shown for the data of low and high resolution phantom experiments, arbitrary multi-planer reformation can be performed, as shown in Figure 8 for four-dimensional flow data of a patient examination. Reformatted color-coded velocity vector fields were overlaid onto corresponding magnitude images in order to visualize aortic output from through- and in-plane perspectives, respectively.

DISCUSSION

Excellent correlation between the established CINE PC methods and our 4D-Flow PC implementation validate our method. Two-dimensional PC was chosen as a comparison because of its extensive application and previous validation in the literature.

In comparison to previous implementations, the whole four-dimensional data set is collected within a single scan covering a true three-dimensional volume, with flexible control of temporal resolution and scan time. Thus, measurements can be performed with high resolution in all spatial dimensions, allowing reformation to arbitrary planes.

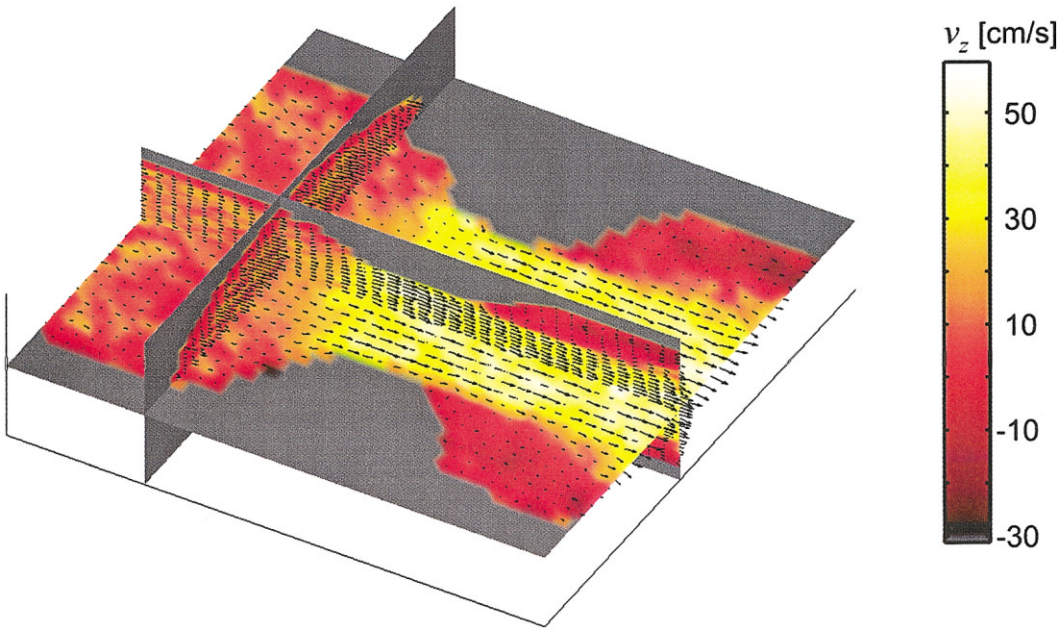

Figure 6. Three-directional velocity vector field in three orthogonal planes inside the acquired three-dimensional volume. Data shown here were collected with a spatial resolution of (0.63 × 0.71 × 1)mm^3. The displayed time frame corresponds to peak flow through the stenotic part of the phantom. The range of the z-components of the measured velocities in the three planes is indicated by the color bar on the right. The velocity outside the segmented phantom was set to zero and was given a gray color to help delineate the lumen boundaries.

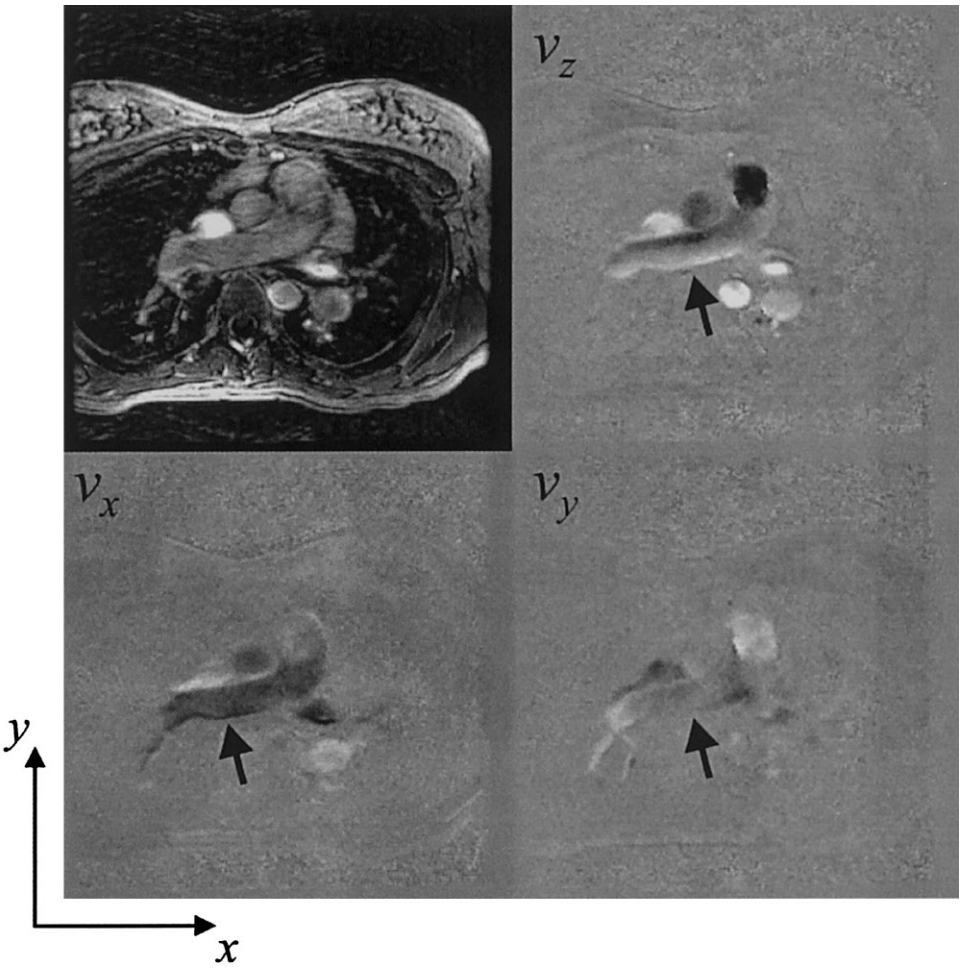

Figure 7. Magnitude (top left) and flow images (top right and bottom row) for an axial slice during systole taken out of a measured three-dimensional volume of a 4D-Flow patient examination. Flow patterns originating from different vessels can be clearly seen on all flow images (v_x, v_y, and v_z). The pulmonary artery (arrows) demonstrates complex and high in-plane flow in the *x*-*y* plane.

The 4D-Flow technique could be successfully applied in human studies using respiratory compensated image acquisition. For normal heart rates, we found the collection of four slice encodes per heart beat to be a reasonable compromise between temporal resolution and total scan time. Although phase reordering techniques for respiratory compensation eliminate ghosting from the resulting images, blurring as a result of the

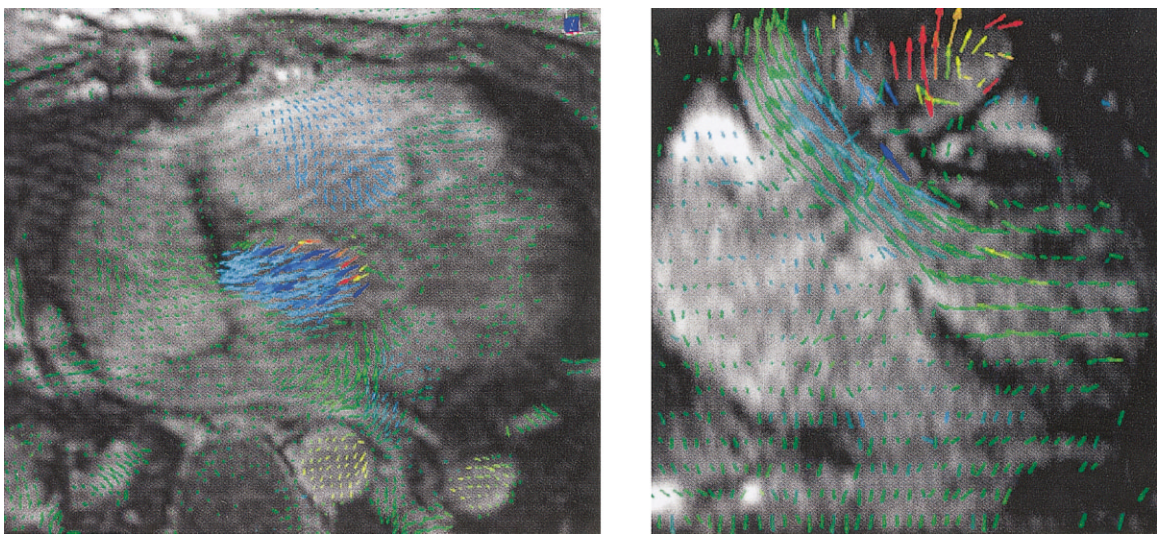

Figure 8. Magnitude-velocity composite images of the aorta at systole. The vector fields represent in-plane velocities, while the color-coding corresponds to through-plane velocities. The mostly transverse image on a level above the aortic valve (left) demonstrates aortic output by high (blue) through-plane velocities. The image on the right shows the aortic output as a vector field in a plane reformatted to the anatomy of the left ventricular outflow tract along the left ventricular long axis and the ascending aorta.

respiratory motion cannot be completely removed. Therefore, the final achievable spatial resolution is limited by the extent of the respiratory motion of the cardiovascular region under investigation. In addition, due to the long total acquisition times, temporal averaging of velocities over a number of cardiac cycles can be expected, and the effects on the measured flow patterns need to be further investigated.

For PC MRI, high SNR is desirable, not only concerning image quality, but also with respect to flow quantification and visualization because it directly affects the noise in the phase-difference images, i.e., in measured flow and velocities. In principle, our time-resolved three-dimensional technique offers a SNR advantage above two-dimensional methods. For non-stationary tissue or in the presence of blood flow entering the imaging slice or volume, however, two-dimensional techniques gain additional SNR due to in-flow enhancement that is mostly absent in the three-dimensional approach.

Such a loss of in-flow enhancement can be compensated for by acquiring data during or after administration of contrast agents using a constant drip of contrast agent over the entire measurement, or, as presented here, with four-dimensional flow imaging performed directly after injection of gadolinium contrast. Due to the long acquisition times, intravascular contrast agents would be best suited for time resolved three-dimensional PC techniques.

Potential improvements of our four-dimensional flow implementation include oblique imaging to adjust the three-dimensional slab for more effective anatomical coverage, and more advanced respiration control techniques. A possible approach consists of introducing a navigator pulse to the pulse sequence to adjust the position of the three-dimensional slab in accordance with the respiratory phase for each cardiac cycle. To handle the large number of images, advanced data processing and display methods are necessary. Development of computer-aided analysis tools is crucial for efficient data extraction, data visualization, and quantitative analysis of the four-dimensional data sets.

ACKNOWLEDGMENTS

The authors would like to thank Gilbert Palafox and Frank Medina from the UTEP W.M. Keck Border Biomedical Manufacturing and Engineering Laboratory for assisting in the development of the phantom models. This work has been supported in part through research collaborations with David Liang (Division of Cardiovascular Medicine, Stanford University).

REFERENCES

1. Moran PR. A flow velocity zeugmatographic interlace for NMR imaging in humans. Magn Reson Imaging 1982;1:197–203.
2. Nayler GL, Firmin DN, Longmore DB. Blood flow imaging by cine magnetic resonance. J Comput Assist Tomogr 1986;10:715–722.
3. Firmin DN, Nayler GL, Kilner PJ, Longmore DB. The application of phase shifts in NMR for flow measurement. Magn Reson Med 1990; 14:230–241.
4. Pelc NJ, Herfkens RJ, Shimakawa A, Enzmann DR. Phase contrast cine magnetic resonance imaging. Magn Reson Q 1991;7:229–254.
5. Pelc NJ, Bernstein MA, Shimakawa A, Glover GH. Encoding strategies for three-direction phase-contrast MR imaging of flow. J Magn Reson Imaging 1991;1:405–413.
6. Bernstein MA, Shimakawa A, Pelc NJ. Minimizing TE in moment-nulled or flow-encoded two- and three-dimensional gradient-echo imaging. J Magn Reson Imaging 1992;2:583–588.
7. Mohiaddin RH, Yang GZ, Kilner PJ. Visualization of flow by vector analysis of multidirectional cine MR velocity mapping. J Comput Assist Tomogr 1994;18:383–392.
8. Bogren HG, Buonocore MH. 4D magnetic resonance velocity mapping of blood flow patterns in the aorta in young vs. elderly normal subjects. J Magn Reson Imaging 1999;10:861–869.
9. Tyszka JM, Laidlaw DH, Asa JW, Silverman JM. Three-dimensional, time-resolved (4D) relative pressure mapping using magnetic resonance imaging. J Magn Reson Imaging 2000;12:321–329.
10. Wigstrom L, Ebbers T, Fyrenius A, et al. Particle trace visualization of intracardiac flow using time-resolved 3D phase contrast MRI. Magn Reson Med 1999;41:793–799.
11. Wigstrom L, Sjoqvist L, Wranne B. Temporally resolved 3D phase-contrast imaging. Magn Reson Med 1996;36:800–803.
12. Fyrenius A, Wigstrom L, Ebbers T, Karlsson M, Engvall J, Bolger AF. Three dimensional flow in the human left atrium. Heart 2001; 86:448–455.
13. Ebbers T, Wigstrom L, Bolger AF, Engvall J, Karlsson M. Estimation of relative cardiovascular pressures using time-resolved three-dimensional phase contrast MRI. Magn Reson Med 2001;45:872–879.
14. Kozerke S, Hasenkam JM, Pedersen EM, Boesiger P. Visualization of flow patterns distal to aortic valve prostheses in humans using a fast approach for cine 3D velocity mapping. J Magn Reson Imaging 2001;13:690–698.
15. Haacke EM, Patrick JL. Reducing motion artifacts in two-dimensional Fourier transform imaging. Magn Reson Imaging 1986;4: 359–376.
16. Cho MH, Kim WS, Cho ZH. CSF flow artifact reduction using cardiac cycle ordered phase-encoding method. Magn Reson Imaging 1990;8:395–405.
17. Napel S, Lee DH, Frayne R, Rutt BK. Visualizing three-dimensional flow with simulated streamlines and three-dimensional phase-contrast MR imaging. J Magn Reson Imaging 1992;2:143–153.
18. Buonocore MH. Visualizing blood flow patterns using streamlines, arrows, and particle paths. Magn Reson Med 1998;40:210–226.
19. Kerr A, Pauly J, Hardy C, Meyer C, Nishimura D, Macovski A. Distributed reconstruction for real-time dynamic MR imaging. In: Proceedings of the 4th Annual Meeting of ISMRM, New York, 1996.
20. Alley MT, Napel S, Amano Y, Paik DS, Shifrin RY, Shimakawa A, Pelc NJ, Herfkens RJ. Fast 3D cardiac cine MR imaging. J Magn Reson Imaging 1999;9:751–755.
21. Amano Y, Herfkens RJ, Shifrin RY, Alley MT, Pelc NJ. Three-dimensional cardiac cine magnetic resonance imaging with an ultrasmall superparamagnetic iron oxide blood pool agent (NC100150). J Magn Reson Imaging 2000;11:81–86.